*Transactions of the Nigerian Association of Mathematical Physics*
*Volume 9,* (*March and May, 2019*), pp111 – 118


# SOLUTION OF THE DISPERSION RELATION FOR MAGNETIZED MULTI-FLUID PLASMA USING PDRF: A CASE STUDY OF MAGNETOSPHERE

*A.M. Nura and A.J. Ado*

**Department of Physics,Bayero University, Kano and Department of Physics, Yusuf Maitama Sule University, Kano, Nigeria.**

***Abstract***

***The magnetosphere is mostly populated by collisionless, anisotropic and inhomogeneous plasma. Wave propagation in plasma can be studied using fluid or kinetic model. In this work the fluid model is applied in solving Plasma dispersion relation for magnetized multi-fluid plasma by employing PDRF code ( Plasma Dispersion Relation Fluid-version). The dispersion relation of some plasma populated region of the magnetosphere was solved by varying plasma $\beta$- value for ions for $k_z \ll k_\perp$. The threshold values of the growth rate were found for $\beta_\perp < \beta_\parallel$ and $\beta_\perp > \beta_\parallel$. As $\beta_\perp$ decrease below $\beta_\parallel$ following a criteria that: $P_\parallel - P_\perp > B_0^2/\mu_0$, the growth rate increases indicating fire hose instability. At $\beta_\parallel = \beta_\perp$, the growth rate was found to be very small indicating transit-time damping. When $\beta_\perp$ increase above $\beta_\parallel$, the growth rate increased indicating mirror instability.***

***Keywords***: Plasma physics, Magnetosphere, Dispersion relation, Multi-Fluid, Waves, Matrix eigenvalue, Instabilities.

## 1.0 Introduction

When the solar wind moves towards the Earth, it impinges on the Earth's dipolarmagnetic field, it is then slowed down and deflected around it, forming a cavity called the magnetosphere [1].Pressure or temperature anisotropy is an important characteristic of collisionless plasma in a strong magnetic field [2] and may develop in the sun, solar wind and planetary magnetospheres, etc for example gyrotropic pressure of $P_\perp > P_\parallel$ and $P_\parallel > P_\perp$ tends to develop in the Earth's magnetosheath and magnetotail, respectively [3, 4]. In the magneto hydrodynamic theory, sufficiently large pressure anisotropy of $P_\perp > P_\parallel$ or $P_\parallel > P_\perp$ may lead to the mirror and fire-hose type instability in a homogeneous magnetized plasma respectively. Instabilities in this regime is considered as velocity space instability at low frequencies ($\omega \ll \omega_{ci}$) as well as at long wavelengths ($\lambda \gg Q_i = {}^{v_T}/_{\omega_{ci}}$) where $\omega_{ci}$is ion cyclotron frequency, $Q_i$ is the ratio of thermal velocity to ion cyclotron frequency of the plasma. It occurs in a high $\beta$ plasma and are caused by anisotropic pressure, where $\beta$is the ratio of plasma kinetic pressure to magnetic pressure [5]. Such instabilities could be treated using MHD equations with anisotropic pressure or kinetic equations. Hasegawa [5] used the kinetic equations to show some significant differences from the results of the MHD equations by introducing a dielectric tensor obtained from the kinetic equations for the hydromagnetic limit: ${k_\perp v_T}/{\omega_{ci}} \sim {\omega}/{\omega_{ci}} \ll 1$, where $k_\perp$ is the wave vector perpendicular to the external magnetic field. In the expressions the effects of wave-particle resonance anisotropic distribution, and existence of relative drift between different species are retained to be used for a study of instabilities.

In this work, we used the general dispersion relation solver PDRF to execute the task of obtaining solutions of dispersion relation

$D(\omega, k) = 0$

for magnetospheric plasma. The solution is obtained for when and where the $\boldsymbol{k}$or$\omega$ are complex. The imaginary part of $\boldsymbol{k}$or $\omega$determines if the oscillations become damped or growing (depending on the sign of the imaginary part). From a mathematical point of view, with perturbation analysis we can study whether an initial perturbation causes undamped oscillations, or whether oscillations are damped or are growing [6]. Here, the firehose and mirror instabilities threshold growth rates were investigated for $\beta_\parallel > \beta_\perp$ and $\beta_\parallel < \beta_\perp$ with $\boldsymbol{k}_\parallel < \boldsymbol{k}_\perp$ respectively. Where,$\boldsymbol{k}_\parallel$ is the wave vector parallel to

Correspondence Author: Nura A.M., Email: nuraa2622@buk.edu.ng, Tel: +2347063517772

the magnetic field, $\boldsymbol{k}_\perp$ is the wave vector perpendicular to the magnetic field, $\beta_\parallel$ and $\beta_\perp$ are the plasma beta-values parallel and perpendicular to the magnetic field respectively.

## 2.0 Theoretical Frame Work

We ignored all temperature gradient effects in the cold multi-fluid plasma, flow velocity of the fluid component j is taken as $v_{j0} = (v_{j0x}, v_{j0y}, v_{j0z})$ in an external static magnetic field $B_0 = (0, 0, B0)$.The species densities are considered to be locally inhomogeneous, with $\nabla n_{j0}/n_0 = (\varepsilon_{njx}, \varepsilon_{njy}, 0) = constant$.The wave vector is assumed to be $k = (k_x, 0, k_z) = (ksin\theta, 0, kcos\theta)$.We use the fluid equations to develop a full dispersion relation matrix and instead of directly solving for its determinant such as that of Swanson[7] or analytical or numerical treatment such as in Stix[8],Ronnmark[9, 10] and Bret [11], we treated it as a matrix eigenvalue problem [12].

The governing equations are the fluid equations:

$$\frac{\partial n_j}{\partial t} = -\nabla \cdot (n_j \boldsymbol{v}_j) \quad (1a)$$

$$\frac{\partial \boldsymbol{u_j}}{\partial t} = -v_j \cdot \nabla \boldsymbol{u}_j + \frac{q_j}{m_j}(\boldsymbol{E} + \boldsymbol{v_j} \times \boldsymbol{B}) - \frac{\nabla \boldsymbol{P}_j}{\rho_j} - \sum_i (\boldsymbol{u_i} - \boldsymbol{u_j}) v_{ij} \quad (1b)$$

$$\frac{\partial \boldsymbol{E}}{\partial t} = c^2 \nabla \times \boldsymbol{B} - \boldsymbol{J}/\epsilon_0 \quad (1c)$$

$$\frac{\partial \boldsymbol{B}}{\partial t} = -\nabla \times \boldsymbol{E} \quad (1d)$$

where $\boldsymbol{u}_j = \gamma_j \boldsymbol{v_j}$, and

$$\boldsymbol{J} = \sum_j q_j n_j \boldsymbol{v}_j \quad (2a)$$

$$\frac{d}{dt}\left(\boldsymbol{P}_{/\!/j} \rho_j^{-\gamma_{/\!/ j}}\right) = 0 \quad (2b)$$

$$\frac{d}{dt}\left(\boldsymbol{P}_{\perp j} \rho_j^{-\gamma_{\perp j}}\right) = 0 \quad (2c)$$

where $\rho_j \equiv m_j n_j, c^2 = 1/\mu_0 \epsilon_0$, $\gamma_j = \left(1 - v_j^2/c^2\right)^{-1/2}$, and $\gamma_{/\!/ j}$ and $\gamma_{\perp j}$are the parallel and perpendicular adiabatic coefficients, respectively.$\boldsymbol{P}_{/\!/\perp} = nT_{/\!/\perp}$,$\boldsymbol{P} = P_{/\!/}\hat{\boldsymbol{b}}\hat{\boldsymbol{b}} + P_\perp(\boldsymbol{I} - \hat{\boldsymbol{b}}\hat{\boldsymbol{b}})$ is anisotropic pressureand $\hat{\boldsymbol{b}} = \boldsymbol{B}/B$. The anisotropy model can be reduced tothat of Bret and Deutsch [13] by setting $\gamma_{/\!/ j} = \gamma_{\perp j} = \gamma_{Tj}$. By further setting $T_{\perp j} = T_{/\!/ j}$, we can recover the isotropic pressure case.

After linearizing, (1) becomes

$$\boldsymbol{J} = \sum_j q_j (n_{j0} v_{j1} + n_{j1} v_{j0}), \quad (3a)$$

$$P_{/\!/,\perp j1} = c^2_{/\!/,\perp j} n_{j1,} \quad (3b)$$

where$c^2_{\parallel,\perp} = \gamma_{\parallel,\perp} P_{\parallel,\perp j0}/\rho_{j0}$ and $P_{j0} = n_{j0} T_{j0}$

we note that

$$\nabla \cdot P_{j1} = (ik_x, 0, ik_z) \begin{vmatrix} P_{\perp j1} & 0 & \Delta_j B_{x1} \\ 0 & P_{\perp j1} & \Delta_j B_{yj1} \\ \Delta_j B_{x1} & \Delta_j B_{y1} & P_{\parallel j1} \end{vmatrix}$$

where$\Delta_j = \left(P_{\parallel j0} - P_{\perp j0}\right)/B_0$ and $\beta_{\parallel,\perp,j} = 2\mu_0 P_{\parallel,\perp j}/B_0^2$. The off-diagonal terms coming from the tensor rotation from $\widehat{b_0}$ to $\hat{b}$ are related to energy exchange and are important for the anisotropic

instabilities. An incorrect treatment or ignoring these off-diagonal terms can cause loss of the firehose and other unstable anisotropic modes.

## 2.1 Matrix Representation

The linearized version of (1) with $g = g_0 + g_1 e^{ik\cdot r - i\omega t}, g_1 \ll g_0$ is equivalent to a matrix eigenvalue problem [11].

$$\lambda \boldsymbol{AX} = \boldsymbol{MX} \quad (4)$$

where$\boldsymbol{X}$ is the eigenvector with$\lambda = -i\omega$asthe eigenvalue and the corresponding eigenvector $\boldsymbol{X}$ also gives the polarization of each normal/eigen mode solution. Same treatments can be found in Hakim [14] for the ten-moment equations and Goedbloed and Poedts [15] for the MHD equations.

Accordingly, we have

$$\boldsymbol{X} = \left(n_{j1}, v_{j1x}, v_{j1y}, v_{j1z}, E_{1x}, E_{1y}, E_{1z}, B_{1x}, B_{1y}, B_{1z}\right)^T,$$

$$u_{j1} = \gamma_{j0}\left[v_{j1} + \gamma_{j0}^2 (v_{j0} \cdot v_{j1})\, v_{j0}/c^2\right] = \{a_{jpq}\} \cdot v_{j1} (p, q = x, y, z), \gamma_{j0} = \left(1 - v_{j0}^2/c^2\right)^{-1/2},$$

And $\boldsymbol{A}$ is given by,

$$\begin{pmatrix} 1 & 0 & 0 & 0 & 0 & 0 & 0 & 0 & 0 & 0 \\ 0 & a_{jxx} & a_{jxy} & a_{jxz} & 0 & 0 & 0 & 0 & 0 & 0 \\ 0 & a_{jyx} & a_{jyy} & a_{jyz} & 0 & 0 & 0 & 0 & 0 & 0 \\ 0 & a_{jzx} & a_{jzy} & a_{jzz} & 0 & 0 & 0 & 0 & 0 & 0 \\ 0 & 0 & 0 & 0 & 1 & 0 & 0 & 0 & 0 & 0 \\ 0 & 0 & 0 & 0 & 0 & 1 & 0 & 0 & 0 & 0 \\ 0 & 0 & 0 & 0 & 0 & 0 & 1 & 0 & 0 & 0 \\ 0 & 0 & 0 & 0 & 0 & 0 & 0 & 1 & 0 & 0 \\ 0 & 0 & 0 & 0 & 0 & 0 & 0 & 0 & 1 & 0 \\ 0 & 0 & 0 & 0 & 0 & 0 & 0 & 0 & 0 & 1 \end{pmatrix}$$

where the relativistic effects in the friction terms $v_{ij}$ are ignored for simplicity. The matrix $\boldsymbol{M}$is given by:

$$\begin{bmatrix} -k \cdot v_{j0} & & & & & & & & & \\ \frac{-k_x c_{\perp j}^2}{\rho_{j0}} & -k_x n_{j0} - \epsilon_{njx} n_{j0} & -\epsilon_{njy} n_{j0} & -ik_z n_{j0} & 0 & 0 & 0 & 0 & -\frac{q_j v_{j0z}}{m_j} & \frac{q_j v_{j0y}}{m_j} \\ 0 & b_{jxx} & b_{jxy} + \omega_{cj} & b_{jxy} & \frac{q_j}{m_j} & \frac{q_j}{m_j} & \frac{q_j}{m_j} & \frac{-ik_z \Delta_j}{m_j n_{j0}} & -\frac{ik_z \Delta_j}{m_j n_{j0}} & -\frac{q_j v_{j0x}}{m_j} \\ \frac{-ik_z c_{/\!/ j}^2}{\rho_{j0}} & b_{jyx} - \omega_{cj} & b_{jyy} & b_{jyz} & 0 & 0 & 0 & \frac{q_j v_{j0z}}{m_j} & \frac{q_j v_{j0x}}{m_j} & 0 \\ -\frac{q_j v_{j0x}}{\epsilon_0} & b_{jzx} & b_{jzy} & b_{jzz} & 0 & 0 & 0 & -\frac{q_j v_{j0y}}{m_j} - \frac{ik_x \Delta_j}{m_j n_{j0}} & -ik_z c^2 & -ik_x c^2 \\ -\frac{q_j v_{j0y}}{\epsilon_0} & \frac{-q_j n_{j0}}{\epsilon_0} & \frac{-q_j n_{j0}}{\epsilon_0} & \frac{-q_j n_{j0}}{\epsilon_0} & 0 & 0 & 0 & 0 & 0 & 0 \\ -\frac{q_j v_{joz}}{\epsilon_0} & 0 & 0 & 0 & 0 & ik_z & ik_x & ik_z c^2 & ik_x c^2 & 0 \\ 0 & 0 & 0 & 0 & -ik_z & 0 & 0 & 0 & 0 & 0 \\ 0 & 0 & 0 & 0 & 0 & -ik_x & 0 & 0 & 0 & 0 \\ 0 & 0 & 0 & 0 & 0 & 0 & 0 & 0 & 0 & 0 \end{bmatrix}$$

where$\omega_{cj} = q_j B_0/m_j$ , $q_e = -e, \omega_{pj}^2 = n_{j0} q_j^2/\epsilon_0 m_j$, and$\{b_{jpq}\} = v_{jj} - i(k \cdot v_{j0}) \cdot \{a_{jpq}\}$.

$$\{a_{jpq}\} \equiv \begin{bmatrix} a_{jxx} & a_{jxy} & a_{jxz} \\ a_{jyx} & a_{jyy} & a_{jyz} \\ a_{jzx} & a_{jzy} & a_{jzz} \end{bmatrix} = \begin{bmatrix} \gamma_{j0} + \gamma_{j0}^3 v_{j0x}^2 / c^2 & \gamma_{j0}^3 v_{j0x} v_{j0y} / c^2 & \gamma_{j0}^3 v_{j0x} v_{j0z} / c^2 \\ \gamma_{j0}^3 v_{j0x} v_{j0y} / c^2 & \gamma_{j0} + \gamma_{j0}^3 v_{j0y}^2 / c^2 & \gamma_{j0}^3 v_{j0y} v_{j0z} / c^2 \\ \gamma_{j0}^3 v_{j0x} v_{j0z} / c^2 & \gamma_{jo}^3 v_{j0y} v_{j0z} / c^2 & \gamma_{j0} + \gamma_{j0}^3 v_{j0z}^2 / c^2 \end{bmatrix} \quad (5)$$

The dimensions of $\boldsymbol{A}$ and $\boldsymbol{M}$ depends on the number of species $s$ of the particles in the plasma. The dimensions is therefore, given as $(4s+6)X(4s+6)$. Without any convergence difficultywe can get all the linear harmonic wave solutions of the system using a standard matrix eigenvalue solver, e.g., the function eig() in MATLAB or LAPACK. Here, a MATLAB code PDRF for solving the above eigenvalue problem wasapplied. By setting $\gamma_j$ to 1, i.e., $\boldsymbol{A} = \boldsymbol{I}$and$\{a_{jpq}\} = \boldsymbol{I}$, PDRF reduces to the non-relativistic case [12].

### 3.0 Program Structure

The program uses two files: an input data file pdrf.in, and function file pdrf.m, for its operation. The program is designed to operate on any computer running MATLAB. Here, a 64-bit MATLAB (R2013b) is used. It is contained in mat.m folder and can be accessed from the command window. The number of lines in the distributed program, pdrf.m including test data is 340 lines, it has a running time of about 1 second on Intel Pentium 2.60GHz PC. It uses a standard matrix Eigenvalue solver, i.e. the function eig() in MATLAB.

The program is designed to use $method = 1$, $method = 2$, $method = 3$ and $method = 4$. When the program is set to $method = 1$, it will generate all the linear harmonic wave solutions of the system without any convergence difficulty. By setting the program to $method = 2$, it will plot dispersion curves $\omega_{r,i}\ versus\ k$ for various values of $\theta$. If the program is set to $method = 3$, it will plot dispersion curves $\omega_{r,i}\ versus\ \theta$ for various values of $k$. When the program is set to $method = 4$, it will plot curves $\omega_{r,i}\ versus\ k_x$ and $k_z$ for range of values of $k_x$ and $k_z$. The input file pdrf.in has the following structure.

| $qs$ | $ms$ | $ns$ | $vsx$ | $vsy$ | $vsz$ | $csz$ | $csp$ | $epsnjx$ | $epsnjz$ |
|---|---|---|---|---|---|---|---|---|---|
| $-1.0$ | 1.0 | 10.0 | 0.0 | 0.0 | 0.0 | 0.0 | 0.0 | 0.0 | 0.0 |
| 1.0 | 1836.0 | 10.0 | 0.0 | 0.0 | 0.0 | 0.0 | 0.0 | 0.0 | 0.0 |

where$qs$ is charge of species, $ms$ is the mass of species, $ns$ is the density of species, $vsx$,$vsy$ and $vsz$ are speed of species in x, y and z directions respectively, $csz$ and $csp$ are sound speeds in parallel and perpendicular direction to the magnetic field respectively. $epsnjx$ and $epsnjy$ are density gradient per unit density of species.

### 3.1 Procedure

Firstly, the parallel and perpendicular sound speeds, $csz$ and $csp$, parallel and perpendicular pressures for low – boundary layer, plasma mantle, tail lobe and plasma sheet were calculated for $\beta_{\parallel i} = 1.0, 0.5, 10^{-4}, 10,\ \beta_{\perp i} \leq \beta_{\parallel i}$and $\beta_{\perp i} \geq \beta_{\parallel i}$ respectively while $\beta_{\parallel,\perp e}$ were set to zero. The MATLAB program code was modified to suit the various parameters for low – boundary layer, plasma mantle, tail lobe and plasma sheet respectively in Table 1. The ratio of parallel to perpendicular wave vector was set to $k_z/k_\perp = 0.01$ to indicate oblique propagation.

**Table 1.Basic parameters for magnetospheric plasmas [16].**

| Plasma parameter | Solar Wind at 1A.U. | Low-latitude Boundary layer | Plasma Mantle | Tail Lobe | Plasma Sheet | Plasmasphere | Polar Wind (low altitude) | Topside Ionosphere |
|---|---|---|---|---|---|---|---|---|
| Number Density $n_i(cm^{-3})$ | 10 | 10 | 1 | $10^{-2}$ | 1 | $10^3$ | 0.1 | $10^4$ |
| Ion Temperature $T_i$ (K) | $10^5$ | $5 \times 10^6$ | $10^6$ | $10^5$ | $5 \times 10^7$ | $10^5$ | $10^5$ | $10^3$ |
| Plasma flow speed $v$ $(kms^{-1})$ | 400 | 200 | 150 | 40 | 10 | 10 | 20 | 0.1 |
| Main Chemical Composition | $H^+, He^{++}$ | $H^+, He^{++}$ | $H^+, He^{++}$ | $H^+, He^+, O^+, N^+$ | $H^+, He^+, O^+, N^+ He^{++}$ | $H^+, He^+, O^+, N^+$ | $H^+, He^+, O^+, N^+$ | $H^+, He^+, O^+, N^+$ |
| Magnetic Field$B(nT)$ | 10 | 40 | 25 | 25 | 10 | $10^3$ | $10^4$ | $10^5$ |
| Scale Length $L$ $(km)$ | $10^8$ | $10^4$ | $10^5$ | $10^5$ | $10^4$ | $10^4$ | $10^4$ | $10^3$ |
| Mean free path $(km)$ | $10^9$ | $10^{12}$ | $10^{12}$ | $10^{10}$ | $10^{15}$ | $10^7$ | $10^{11}$ | $10^2$ |
| Thermal ion gyroradius $(km)$ | $10^2$ | $10^2$ | $10^2$ | $10^2$ | $10^3$ | 1 | 0.1 | $10^{-3}$ |
| Plasma beta$\beta$ | 0.5 | 1 | 0.5 | $10^{-4}$ | 10 | $10^{-3}$ | $10^{-9}$ | $10^{-8}$ |

Secondly, the input data file of the PDRF code was then modified to suit $csp$,$csz$ and $ns$ for the plasma populated region of the magnetosphere.The PDRF code was also modified to$rel = 0$ which reduce it to non relativistic case, with$m_i/m_e = 1836$and $\gamma = 5/3$for ideal gas [14].Where, all parameters still maintain their usual meanings.

Thirdly, on the command window, a call to**pdrf** will generate all the linear harmonic wave solutions of the system without any convergence difficulty using $method = 1$.

Fourthly, the threshold values of the complex part, $\omega_i$ of the solution were obtained for both with and without correction. Threshold values for the growth rate were plotted for $\beta_\parallel < \beta_\perp$and $\beta_\parallel > \beta_\perp$.

### 4.0 Results and Discussion

The solutions of the dispersion relations of the magnetospheric plasma are given in forms of graphs. Figures 1.1- 1.5 show the graphs of growth rate against $\beta_\perp$ for curves of (I) $\beta_{\perp i} < \beta_{\parallel i}$and (II) $\beta_{\perp i} > \beta_{\parallel i}$ for constant value of $\beta_{\parallel i}$ (with correction and without correction) for firehose and mirror instability.

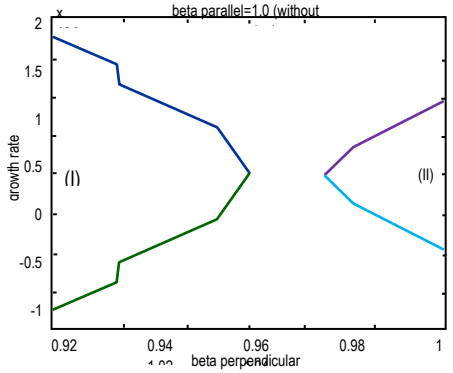


1.1 (a)

Fig. 1.1a. The graph of growth rate against $\beta_\perp$ for curves (I)$\beta_{\perp i} < \beta_{\parallel i}$and (II) $\beta_{\perp i} > \beta_{\parallel i}$ for constant value of $\beta_{\parallel i} = 1$ (without correction) for low-latitude boundary of magnetosphere for firehose and mirror instability thresholds respectively, with $B_0 = 40nT$, $n_i = 10cm^{-3}$ and $\beta = 0.5$.

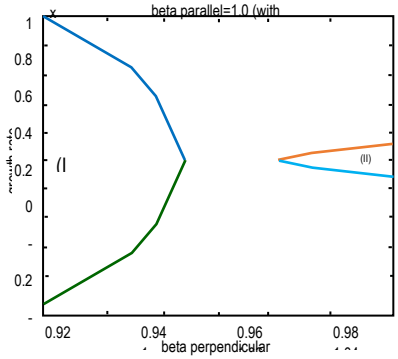


1.1 (b)

Fig. 1.1b. The graph of growth rate against $\beta_\perp$ for curves (I)$\beta_{\perp i} < \beta_{\parallel i}$and (II) $\beta_{\perp i} > \beta_{\parallel i}$for constant value of $\beta_{\parallel i} = 1$ (with correction) for low-latitude boundary of magnetosphere for firehose and mirror instability thresholds respectively, with $B_0 = 40nT$, $n_i = 10cm^{-3}$ and $\beta = 0.5$

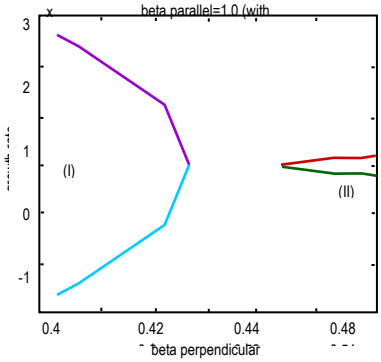


1.2 (a)

Fig. 1.2a. The graph of growth rate against $\beta_\perp$ for curves (I)$\beta_{\perp i} < \beta_{\parallel i}$and (II) $\beta_{\perp i} > \beta_{\parallel i}$ for constant value of $\beta_{\parallel i} = 0.5$ (with correction) for plasma mantle of magnetosphere for firehose and mirror instability thresholds respectively, with $B_0 = 25nT$, $n_i = 1cm^{-3}$ and $\beta = 0.5$.

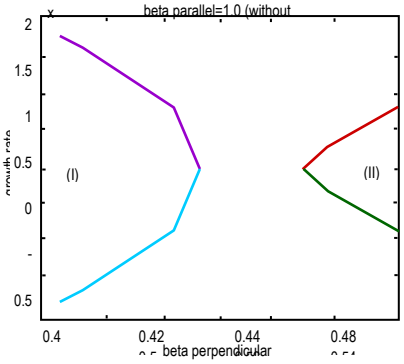


1.2 (b)

Fig. 1.2b. The graph of growth rate against $\beta_\perp$ for curves (I)$\beta_{\perp i} < \beta_{\parallel i}$and (II) $\beta_{\perp i} > \beta_{\parallel i}$ for constant value of $\beta_{\parallel i} = 0.5$ (without correction) for plasma mantle of magnetosphere for firehose and mirror instability thresholds respectively, with $B_0 = 25nT$, $n_i = 1cm^{-3}$ and $\beta = 0.5$.

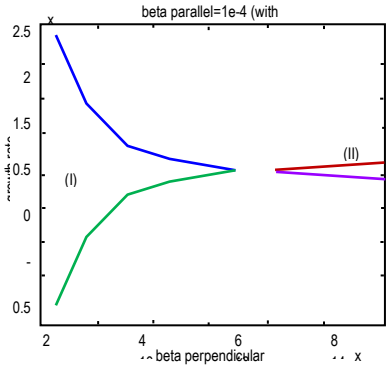


1.3 (a)

Figure 1.3a. The graph of growth rate against $\beta_\perp$ for curves (I)$\beta_{\perp i} < \beta_{\parallel i}$and (II) $\beta_{\perp i} > \beta_{\parallel i}$ for constant value of $\beta_{\parallel i} = 10^{-4}$ (with correction) for tail lobe of magnetosphere for firehose and mirror instability thresholds respectively, with $B_0 = 25nT$, $n_i = 10cm^{-3}$ and $\beta = 1 \times 10^{-4}$.

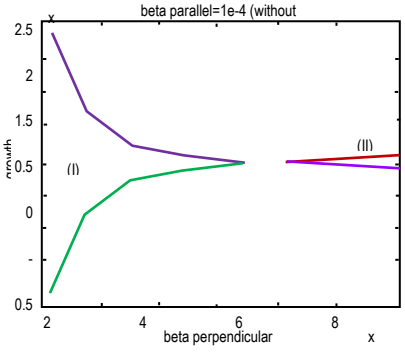


1.3 (b)

Figure 1.3b. The graph of growth rate against $\beta_\perp$ for curves (I)$\beta_{\perp i} < \beta_{\parallel i}$and (II) $\beta_{\perp i} > \beta_{\parallel i}$for constant value of $\beta_{\parallel i} = 10^{-4}$ (without correction) for tail lobe of magnetosphere for firehose and mirror instability thresholds respectively, with $B_0 = 25nT$, $n_i = 10cm^{-3}$ and $\beta = 1 \times 10^{-4}$.

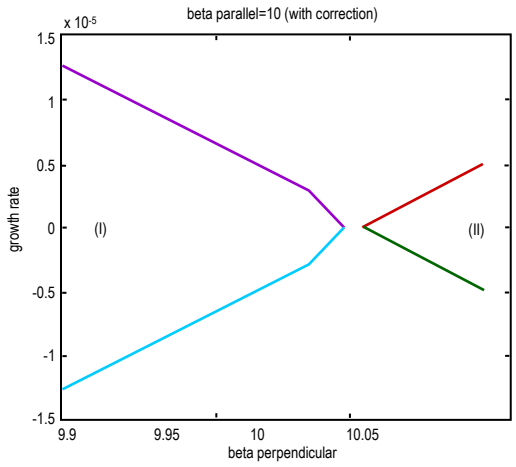


1.4 (a)

Fig. 1.4a. The graph of growth rate against $\beta_\perp$ for curves (I)$\beta_{\perp i} < \beta_{\|i}$and (II) $\beta_{\perp i} > \beta_{\|i}$for constant value of $\beta_{\|i} = 10$ (with correction) for plasma sheet of magnetosphere for firehose and mirror instability thresholds respectively, with $B_0 = 10nT$, $n_i = 1cm^{-3}$ and $\beta = 10$.

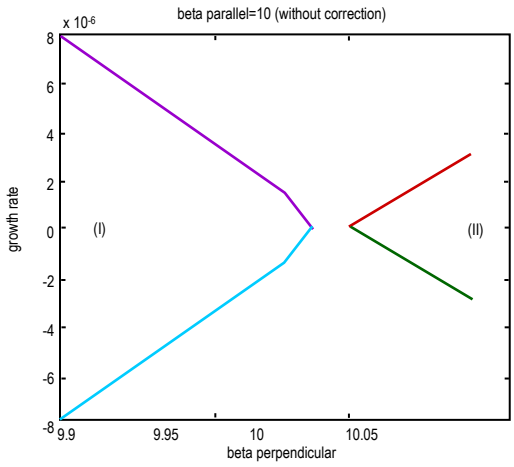


1.4 (b)

Fig. 1.4b. The graph of growth rate against $\beta_\perp$ for curves (I)$\beta_{\perp i} < \beta_{\|i}$and (II) $\beta_{\perp i} > \beta_{\|i}$ for constant value of $\beta_{\|i} = 10$ (without correction) for plasma sheet of magnetosphere for firehose and mirror instability thresholds respectively, with $B_0 = 10nT$, $n_i = 1cm^{-3}$ and $\beta = 10$.

Figures 1.5(a-b) are the solutions of the test problem which was obtained and plotted.

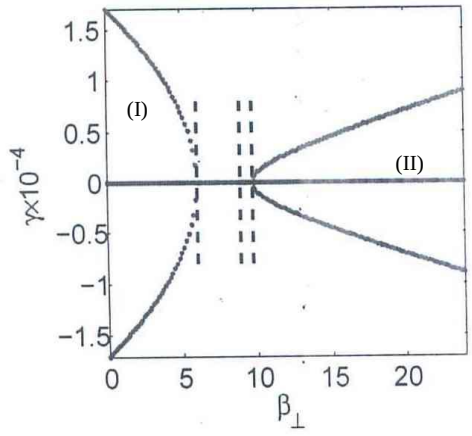


1.5 (a)

Figure 1.5(a). (I) The firehose and (II) mirror instability thresholds for a test problem with correction for $\beta_{\|i} = 8$ and $\beta_{\|,\perp e} = 0$ by Xie [12]. The dots indicate theoretical prediction.

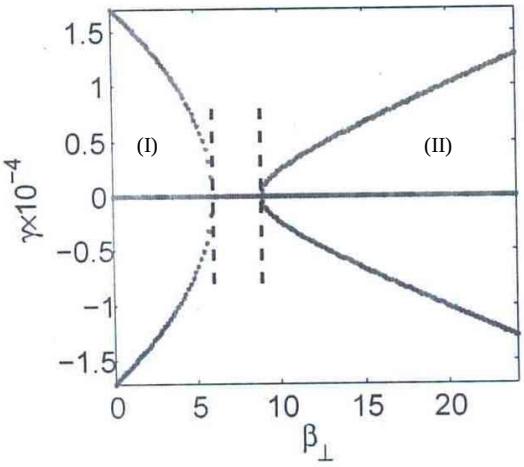


1.5 (b)

Figure 1.5(b). (I) Firehose and (II) mirror instability thresholds for a test problem without correction for $\beta_{\|i} = 8$ and $\beta_{\|,\perp e} = 0$ by Xie [12]. The dots indicates theoretical predictions

In Figures 1.1a and 1.1b the lowest value of the growth rate obtained was $1.03 \times 10^{-9} s^{-1}$at a point where $\beta_{\parallel} = \beta_{\perp} = 1.0$ with a sound speed $c_{\parallel} = c_{\perp} = 2.40 cms^{-1}$ and pressure of $P_{\parallel} = P_{\perp} = 6.35 \times 10^{4} dyn\ per\ cm^{2}$ for both with and without correction. At $\beta_{\perp} = \beta_{\parallel}$ the solution has the same value of growth rate both with correction and without correction, according to Stix [13] this represent the transit time damping which is characterized by isotropic pressure of $P_{\perp} = P_{\parallel}$ , which was generated by a sound speed of $C_{\perp} = C_{\parallel}$. The transit-time damping is the magnetic analogue of Landau damping where $\mu B_{\parallel}$ acts like an electrostatic potential $\varphi$, where $\mu$ is the magnetic moment.

As $\beta_{\perp}$ decreases below $\beta_{\parallel}$ by greater than 2, the growth rate began to increase indicating firehose instability. The growth rate reached a value of about $9.82 \times 10^{-5} s^{-1}$ with correction and without correction was $1.75 \times 10^{-5} s^{-1}$ for a sound speed of $c_{\perp} = 2.31 cms^{-1}$ and a pressure of $P_{\perp} = 5.84 \times 10^{4} dyn\ per\ cm^{2}$. At $\beta_{\parallel} > \beta_{\perp}$ the parallel thermal pressure in the plasma is sufficiently high. The magnetic flux become unstable for transverse oscillations of the magnetic field and at the same time excites parallel propagating Alfvén waves. Therefore as $\beta_{\perp}$ becomes small for larger $\beta_{\parallel}$ by a difference of 2, the incompressible fire hose instability sets in as the growth rate increases with decrease in $\beta_{\perp}$. The firehose instability is a non-oscillating, purely growing mode. This result from the parallel thermal pressure in the magnetohydrodynamic fluid being sufficiently high by $P_{\parallel} - P_{\perp} > {B^2}/{\mu_0}$, the magnetic flux tubes become unstable for transverse oscillations of the magnetic field and spontaneously excite parallel propagating Alfvén waves. In the magnetohydrodynamic approximation, where these waves are non-dispersive, the wave has no real frequency and is a very-low frequency wave in the lowest part of the Alfvén branch [18].

The firehose instability is a very strong instability, but it requires large parallel pressure or $\beta_{\parallel} > 2$, which implies that the instability is possible only in high-beta or low magnetic field plasmas as, for instance, in the solar wind. This region may therefore become spontaneously excited to release fast growing Alfvén waves with amplitudes which are large. Once excited, the oscillation will propagate as an Alfvén wave along the magnetic field lines into the near-Earth magnetosphere.The physical mechanism of thisinstability is similar to that which generates oscillations in a water hosewhen the water pressure exceeds a critical value[5].

As $\beta_{\perp}$ increases greater than$\beta_{\parallel}$, the growth rate began to increase indicating mirror instability. Highest growth rate value obtained for a sound speed of $c_{\perp} = 2.45 cms^{-1}$ and a pressure of $P_{\perp} = 6.60 \times 10^{4} dyn\ per\ cm^{2}$ are $1.40 \times 10^{-5} s^{-1}$ with correction and $9.93 \times 10^{-6} s^{-1}$ without correction.Ideally when a compressional wave is set up, it is ordinarily damped out by the transit time damping at $\beta_{\perp} = \beta_{\parallel}$ . However, when $\beta_{\perp} > \beta_{\parallel}$ , the diamagnetic repulsion of the plasma, which is trapped in the local mirror field created by the wave, excludes the magnetic field. This instability causing a local deformation of the magnetic field makes the plasma spatially inhomogeneous. It occurs because a part of the particles captured in "weak mirror traps" subdivides the distribution of particles into passing and trapped species. This accelerates the flow of plasma into the deepened well of the local mirror, and therefore the perturbation grows as $\beta_{\perp} \gg \beta_{\parallel}$ [5].

In Figures 1.2a and 1.2b the lowest value of the growth rate obtained was $2.73 \times 10^{-8} s^{-1}$at a point where $\beta_{\parallel} = \beta_{\perp} = 0.5$ with a sound speed $c_{\parallel} = c_{\perp} = 3.36 cms^{-1}$ and pressure of $P_{\parallel} = P_{\perp} = 1.24 \times 10^{4} dyn\ per\ cm^{2}$ for both with and without correction. As $\beta_{\perp}$ decreases below $\beta_{\parallel}$ by greater than 2, the growth rate began to increase indicating firehose instability. The growth rate reached a value of about $2.44 \times 10^{-4} s^{-1}$ with correction and without correction was $1.73 \times 10^{-5} s^{-1}$ for a sound speed of $c_{\perp} = 3.05 cms^{-1}$ and a pressure of $P_{\perp} = 1.02 \times 10^{4} dyn\ per\ cm^{2}$. As $\beta_{\perp}$ increases greater than$\beta_{\parallel}$, the growth rate began to increase indicating mirror instability. Highest growth rate value obtained for a sound speed of $c_{\perp} = 3.49 cms^{-1}$ and a pressure of $P_{\perp} = 1.34 \times 10^{4} dyn\ per\ cm^{2}$ are $1.09 \times 10^{-5} s^{-1}$ with correction and $7.74 \times 10^{-6} s^{-1}$ without correction.

In Figures 1.3a and 1.3b the lowest value of the growth rate obtained was $8.82 \times 10^{-10} s^{-1}$at a point where $\beta_{\parallel} = \beta_{\perp} = 1.0 \times 10^{-4}$ with a sound speed $c_{\parallel} = c_{\perp} = 4.75 \times 10^{-1} cms^{-1}$ and pressure of $P_{\parallel} = P_{\perp} = 2.48\ dyn\ per\ cm^{2}$ for both with and without correction. As $\beta_{\perp}$ decreases below $\beta_{\parallel}$ by greater than 2, the growth rate began to increase indicating firehose instability. The growth rate reached a value of about $2.33 \times 10^{-7} s^{-1}$ with correction and without correction was $2.34 \times 10^{-7} s^{-1}$ for a sound speed of $c_{\perp} = 2.38 \times 10^{-1} cms^{-1}$ and a pressure of $P_{\perp} = 0.62\ dyn\ per\ cm^{2}$. As $\beta_{\perp}$ increases greater than$\beta_{\parallel}$, the growth rate began to increase indicating mirror instability. Highest growth rate value obtained for a sound speed of $c_{\perp} = 5.62 \times 10^{-1} cms^{-1}$ and a pressure of $P_{\perp} = 3.47\ dyn\ per\ cm^{2}$ are $1.15 \times 10^{-8} s^{-1}$ with correction and $8.14 \times 10^{-9} s^{-1}$ without correction.

In Figures 1.4a and 1.4b the lowest value of the growth rate obtained was $5.47 \times 10^{-8} s^{-1}$at a point where $\beta_{\parallel} = \beta_{\perp} = 10$ with a sound speed $c_{\parallel} = c_{\perp} = 6.01 cms^{-1}$ and pressure of $P_{\parallel} = P_{\perp} = 3.97 \times 10^{4}\ dyn\ per\ cm^{2}$ for both with and without correction. As $\beta_{\perp}$ decreases below $\beta_{\parallel}$ by greater than 2, the growth rate began to increase indicating firehose instability. The growth rate reached a value of about $1.12 \times 10^{-5} s^{-1}$ with correction and without correction was $7.92 \times 10^{-6} s^{-1}$ for a sound speed of $c_{\perp} = 5.9802 cms^{-1}$ and a pressure of $P_{\perp} = 3.93 \times 10^{4}\ dyn\ per\ cm^{2}$. As $\beta_{\perp}$ increases greater than$\beta_{\parallel}$, the growth rate began to increase indicating mirror instability. Highest growth rate value obtained for a sound speed of $c_{\perp} = 6.0226 cms^{-1}$ and a pressure of $P_{\perp} = 3.98 \times 10^{4}\ dyn\ per\ cm^{2}$ are $4.44 \times 10^{-6} s^{-1}$ with correction and $3.14 \times 10^{-6} s^{-1}$ without correction.

Figures 1.5a and 1.5b are the solutions of the test problem which was obtained and plotted. We see that ingeneral the numerical and analytical results agree. The test problem was used as guide to arrive at the solutions in Figures 1.1 – 1.4. In the test problem, the damping of the growth rate was fast in the fire hose instability curve while in the mirror instability curve the damping was slow compared to that of the magnetosphere. This might have resulted due to difference in parameters used for each case.

## 5.0 Conclusion

We have solved the dispersion relation for the fire hose and mirror growth rates with and without correction using the PDRF for the various plasma populated regions of the magnetosphere. We have found that the results obtained were in accordance with that obtained from previous literature.

We recommend that the kinetic model should be used to solve the dispersion relation. The PDRF code could be used to verify test data from satellites. It could also be used to solve dispersion relation in warm plasma, unmagnetized plasma (by setting $B_0 = 0$) and to study magnetospheres of different planets rather than just ours which is Earth.

## References

[1] Richard, A. M. (2001). Dictionary of geophysics, Astrophysics and Astronomy, CRC Press, LLC, Corporate Blvd. Baton, Florida 33431.

[2] Chew, G. F., Goldberger, M. L. and Low, F. E. (1956). The Boltzmann equation and the one-fluid hydromagnetic equations in the absence of particle collisions. Proc. R. Soc. London, Ser A, 236: 112.

[3] Li, X., Lewis, H. R., LaBelle, J., Phan, T. D. and Treumann, R. A. (1995).Characteristics of the ion pressure tensor in the earth's magnetosheath. Geophys.Res. Lett., 22: 667– 670.

[4] Kaufmann, R., Lu, C., Paterson, W. R and. Frank, L. A. (2002). Three-dimensional analysis of electric currents and pressure anisotropies in the plasma sheet. J. Geophys. Res., 107 (A7): 1103.

[5] Hasegawa, A. (1975). Plasma Instabilities and Nonlinear Effects. 1st ed., New York: Springer-Verlag. Vol. 8.

[6] Kulhánek, P. (2011) *Úvod do teorieplazmatu*. AGA, 1st. edition. In Czech language only.

[7] Swanson, D. G. (2003). Plasma Waves. Second edition, U.S.A.: IOP., (Series in plasma physics).

[8] Stix, T. (1992).Waves in Plasma. New York: AIP Press.

[9] Ronnmark, K. (1982). Waves in Homogeneous, Anisotropic, Multi-fluid Plasmas. Kiruna Geophysical Institute Reports, 179.

[10] Ronnmark, K. (1983). Computation of the dielectric tensor of a Maxwellian plasma. Plasma Phys., 25: 699.

[11] Bret, A. (2007). Beam plasma dielectric tensor with mathematica, Computer Phys. Comm., 179: 362.

[12] Xie, H. S. (2013). PDRF: A general dispersion relation solver for magnetized multi-fluid plasmas. Computer Physics Communications, 185: 670 - 675.

[13] Bret, A. and Deutsch, C. (2006). A fluid approach to linear beam plasma electromagnetic instabilities. Phys. Plasmas, 13: 042106.

[14] Hakim, A. (2008). Towards closures for multi- fluid moment simulations of cllisionles plasmas. J. Fusion Energy, 27: 36.

[15] Goedbloed, J. and Poedts, S. (2004). Principles of Magnetohydrodynamics: With Applications to Laboratory and Astrophysical Plasmas. New York: Cambridge University Press.

[16] Priest, E. R. and Wood, A. W. (1991). Advances in solar system magnetohydrodynamics. Cambridge university press, Cambridge, New York. P. 368.

[17] Stix, T. (1962). The theory of plasma waves. New York: McGraw Hill.

[18] Baumjohann, W. and Treumann, R. A. (1996). Basic Space Plasma Physics. London: Imperial College Press.